Steel and Composite Structures, *Vol. 34, No. 5 (2020) 625-641*
DOI: https://doi.org/10.12989/scs.2020.34.5.625

Behavior of semi-rigid steel frames under near- and far-field earthquakes

Vijay Sharma*[1], Mahendra K. Shrimali[2a], Shiv D. Bharti[2b] and Tushar K. Datta[2c]

[1]*Department of Civil Engineering, Malaviya National Institute of Technology Jaipur, JLN Marg, Jaipur 302017, India*
[2]*National Centre for Disaster Mitigation and Management, Malaviya National Institute of Technology Jaipur, JLN Marg Jaipur, 302017, India*

(*Received March 29, 2019, Revised October 28, 2019, Accepted December 30, 2019*)

Abstract. The realistic modeling of the beam-column semi-rigid connection in steel frames attracted the attention of many researchers in the past for the seismic analysis of semi-rigid frames. Comparatively less studies have been made to investigate the behavior of steel frames with semi-rigid connections under different types of earthquake. Herein, the seismic behavior of semi-rigid steel frames is investigated under both far and near-field earthquakes. The semi-rigid connection is modeled by the multilinear plastic link element consisting of rotational springs. The kinematic hysteresis model is used to define the dynamic behavior of the rotational spring, describing the nonlinearity of the semi-rigid connection as defined in SAP2000. The nonlinear time history analysis (NTHA) is performed to obtain response time histories of the frame under scaled earthquakes at three PGA levels denoting the low, medium and high-level earthquakes. The other important parameters varied are the stiffness and strength parameters of the connections, defining the degree of semi-rigidity. For studying the behavior of the semi-rigid frame, a large number of seismic demand parameters are considered. The benchmark for comparison is taken as those of the corresponding rigid frame. Two different frames, namely, a five-story frame and a ten-story frame are considered as the numerical examples. It is shown that semi-rigid frames prove to be effective and beneficial in resisting the seismic forces for near-field earthquakes (PGA $\approx$ 0.2g), especially in reducing the base shear to a considerable extent for the moderate level of earthquake. Further, the semi-rigid frame with a relatively weaker beam and less connection stiffness may withstand a moderately strong earthquake without having much damage in the beams.

Keywords: nonlinear time history analysis; semi-rigid steel frame; near-field; far-field earthquakes

1. Introduction

Properly designed multistorey steel frames are efficacious under seismic excitations due to their capability in the dissipation of seismic energy through the damping and large inelastic deformation characteristics. Due to this reason, steel frames are preferred in seismically active regions. For the seismic analysis and design of steel frames, there exist several codes of practice. However, the code provisions cater mostly to the far-field earthquakes. For the near-field earthquakes, definite guidelines have not yet been codified. Various researches in this direction are continuing to study the dynamic behavior of steel frames in near-fault zone.

Seismic activities within 20 km distance from the rupture fault are considered as the near-field or near-fault ground motions. The near-fault ground motions are usually characterized by the high amplitude, long period velocity and displacement pulses that precisely distinguish them from the far-field (> 20 km) ground motions. The characteristics of the near-field ground motions were first observed in the 1966 Parkfield, California earthquake and were described by Housner and Trifunac (1967). Later on, severe damages to flexible structures in the near-fault ground motions during the 1971 San Fernando earthquake were observed by Bertero *et al.* (1978). It was for the first time that the seismic engineers realized the great impact of the impulsive nature of the near-fault ground motion on structures. During the 1994 Northridge, California and 1995 Kobe, Japan earthquakes, the steel moment-resisting frames with welded connections were severely damaged. These observations also made the seismic engineers aware of the severity and destructive potential of the near-field ground motion pulses in urban areas.

In the near-field region, the earthquakes at particular sites are greatly influenced by the fault rupture mechanism, slip direction relative to the rupture and permanent ground displacement at the site relative to the residual tectonic displacement. Based on the above factors, the near-field effect can be categorized into two types, namely, the directivity effect (forward, backward or neutral) and the fling-step effect. If the rupture front propagates toward the site, and the direction of slip on the fault is aligned with a site, the effect of the forward directivity takes place in near-field regions. On the other hand, if the rupture front

*Corresponding author, Ph.D. Student
E-mail: vrsgec2011@gmail.com
[a]Professor
E-mail: shrimalimk@gmail.com
[b]Professor
E-mail: sdbharti@mnit.ac.in
[c]Professor
E-mail: tushar_k_datta@yahoo.com

http://www.techno-press.org/?journal=scs&subpage=6
ISSN: 1229-9367 (Print), 1598-6233 (Online)

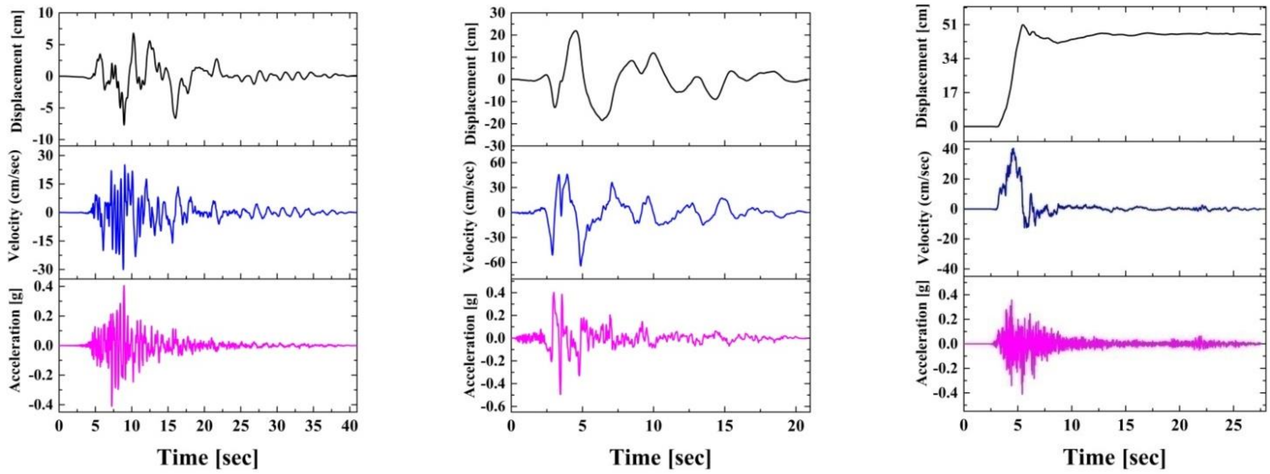

(a) FF Kobe earthquake (b) NFD Erzincan earthquake (c) NFF Kocaeli earthquake

Fig. 1 Typical characteristics of far-field, near-field with directivity effect, and near-field with fling-step effect earthquakes

propagates away from the site, it results in the backward directivity effect. The forward directivity can be met in both strike-slip and dip-slip fault mechanisms. The forward directivity effect has a two-sided pulse in the velocity time history and does not have permanent tectonic displacement (Somerville *et al.* 1997). The fling-step effect is a result of the permanent static displacement of the fault and has a one-sided pulse in the velocity time history. Li and Xie (2007) extensively reviewed the state-of-the-art problems related to the influence of near-field ground motions on structures. Various researchers studied the relationships between the PGA, PGV, PGD and pulse period T_v in near-field pulse characteristics (Malhotra 1999, Huang 2003, Bray and Rodriguez-Marek 2004). Recently, a pulse identification criterion was developed to identify the pulse type directivity motion or nonpulse motion, based on the maximum fractional energy contributed by a half cycle in the velocity time-history. The characterization of the theory is based on the superposition of one or more pulse-type motions over the nonpulse motions. Further, the scaling method for modeling the primary, and the link between the primary and secondary pulses were derived considering the characteristics of directivity parameters, earthquake moment magnitude and closest distance for the pulse amplitude and pulse period (Mukhopadhyay and Gupta 2013, Mukhopadhyay and Gupta 2013). The importance of the 3D waveform modeling for the near-field with fling step earthquakes was predicted after studying the 1999 Chi-Chi earthquake characteristics by (Wang *et al.* 2002). A mathematical model was proposed to characterize and simulate the fling step pulses into a pulse component and without a pulse component considering the amplitude, duration, and location of the pulse (Yadav and Gupta 2017). (Foti 2014) studied the effects of near-field ground motions on frame structures and assessed the damage pattern using the passive seismic systems. (Foti 2014) investigated the seismic response of mid-rise braced steel frames under the far-field and near-field earthquakes. The local soil effects on seismically protected concrete buildings under far-field and near-field earthquakes were studied using diagonal steel energy dissipater braces by Foti (2015).

Fig. 1 exhibits the comparison in characteristics among the far-field (FF), near-field with directivity effect (NFD) and near-field with fling-step effect (NFF) by the corresponding displacement, velocity and acceleration time histories. It is apparently observed that the near-field earthquakes have a long duration pulse which occurs near the beginning of the ground velocity and displacement time histories (Archuleta and Hartzell 1981). Figs. 1(b) and 1(c) shows that the NFD has two-sided pulses, whereas the NFF has a one-sided pulse in the velocity and displacement time histories and permanent ground displacement.

Previous studies had shown that the pulse type excitations increased the severity of the seismic demand on multistorey structures (Hall *et al.* 1995, Heaton *et al.* 1995). Alavi and Krawinkler (2004) investigated the vulnerability of intermediate period structures under the forward directivity pulses and suggested strengthening techniques to reduce the seismic demand in multistorey structures. Kalkan and Kunnath (2006) investigated the repercussion of the directivity and fling characteristics of near-fault ground motions on the seismic demands of steel moment frames and the effect of high-amplitude pulses on the structural demands by considering idealized pulses. Sehhati *et al.* (2011) evaluated the seismic demands of three multistorey structures (low, mid and high rise) subjected to the near-fault directivity and far-fault ground motions using an incremental dynamic analysis approach considering the damping and P-Delta effects. Davoodi *et al.* (2012) studied the effect of the near-fault and far-fault ground motions considering the soil-structure interaction in the soft soil to evaluate the maximum response of an SDOF system. Asgarian *et al.* (2012) investigated the effect of the vertical component of near-field earthquakes accompanied with the horizontal component for seismic performance evaluation of moment resistant frames as per FEMA 350 guidelines. Abdollahzadeh *et al.* (2016) studied the dissipation of hysteretic energy and variation of inter-story drift in steel V-brace building subjected to the far-field and near-field earthquakes. Diaferio (2018) investigated the seismic performance of the shear panels in MRFs under the near-field ground motions in the form of the hysteretic energy dissipation and shear stress evaluation. Shahbazi *et al.* (2019) carried out a comparative study considering the effect of the vertical component of the far-field and near-field with forward directivity effect on the seismic performance of steel rigid frames.

From the previous studies on steel rigid frame structures under the near-field and far-field ground motions, it was found that beam-column connections played a vital role to minimize the responses. During the 1994 Northridge and 1995 Kobe earthquakes, the beam-column welded connected steel frames were severely damaged, and the research interest was inclined toward the partially restrained or semi-rigid (SR) connections. The most codes of practice, including the Indian Standard (IS-1893 2016) also accounted for all three types of beam-column connections. Díaz *et al.* (2011) made an extensive state-of-art review of the semi-rigid (SR) connections to study the moment-rotation (M-Φ) behavior based on various models such as the analytical, experimental, empirical, mechanical, informational, and numerical models. Frye and Morris (1975) presented the polynomial function which depends on the connection type, geometry and curve-fitting constants for different SR connections. Various other polynomial models are also available like an exponential model (Lui and Chen 1987) and a modified exponential model (Kishi and Chen 1990). Fang *et al.* (2013) presented a component approach of modeling of semi-rigid connections based on Eurocode 3 for severe loading. Faridmehr *et al.* (2016) studied SR connections by investigating the strength, stiffness, and ductility by ANSI/AISC-341 (2010) and Mavroeidis *et al.* (2004) specifications.

Under the seismic excitation, the SR connection can dissipate energy in the hysteresis loop without significant damage. Nader and Astaneh (1991) studied the single-story steel frame with all three types of connections at different PGA levels and found that well-proportioned SR connections increase the dynamic performance in low rise structures. Al-Bermani *et al.* (1994) presented the hysteretic M-θ behavior of SR or flexible joints using the two-joint zero-length element to model the nonlinear response of the connection under the cyclic and dynamic loading. Elnashai and Elghazouli (1994) investigated experimentally and analytically the performance of SR connected steel frames in terms of the extent of plastification under seismic excitation. Della Corte *et al.* (2002) presented a mathematical hysteresis model of beam-column joints to account for the strength degradation and pinching in connection to the behavior, in place of the conventional elastic-perfectly-plastic hysteretic model subjected to the near-fault ground motion. Fathi *et al.* (2006) reviewed the existing method to estimate the behavior factor (R) or response reduction factor for the rigid, and SR connected moment-resisting steel frames, limited to 10 stories and five-span frames, and proposed a modified method to estimate the reduction factor considering the earthquake resistance and energy dissipation capacity under the design level earthquake. Aksoylar *et al.* (2011) investigated the design and seismic performance of low-rise large span SR frames with variation in the moment-hardening ratio, semi-rigid connection capacities, connection hysteretic curve subjected to an ensemble of strong near-fault and far-fault ground motions. Najdian and Izadinia (2012) compared the behavior of rigid and semi-rigid connected frames under the near-fault ground motion and reported improved performance of semi-rigid frames, especially in short duration high energy pulse type excitations. Mahmoud *et al.* (2013) investigated experimentally and analytically the seismic performance of SR connected steel frames in terms of local and global demands under the near-field and far-field earthquakes. Daryan *et al.* (2014) investigated the seismic behavior of semi-rigid steel frames and observed that the increased shear stiffness significantly decreased the drift capacity of the frame and enhanced the frame stability against lateral forces. Stamatopoulos (2014) examined the behavior of SR column base plate steel frames under the fault normal seismic excitation having a large velocity pulse. Feizi *et al.* (2015) studied with a different location and combination of SR connections for the 3, 8 and 15 story hybrid or dual frames and found that the dual-frame performance was significantly better than the rigid frame, and the frame behavior was more dependent on the moment capacity of the connection for the ultimate limit state. Diaferio and Foti (2016) investigated the mechanical behavior of semi-rigid steel frames with different stiffness properties under near-field ground motions. Recently, Bayat and Zahrai (2017) investigated the seismic performance and best pattern and location of the 10, 15 and 20 story hybrid SR frames and compared responses with those obtained from rigid frames under severe far-field ground motions. A nonlinear stiffness matrix method was proposed to assess the seismic response of SR steel frames, and numerical results were compared between the rigid and SR frames under a set of earthquakes by Faridmehr *et al.* (2017). The research studies showed that SR connected frames were economical due to the less base shear demand and high interstorey drift capacity. Lemonis (2018) and Sharma *et al.* (2019) examined the seismic performance of special moment resisting frames analytically in the context of energy dissipation in joints and beams.

A review of the previous research studies showed that although considerable studies have been made on the behavior of SR connected steel frames under both near and far-field earthquakes, a comprehensive study on the comparative behavior of SR frames under NFF, NFD and FF ground motions is lacking. Further, different seismic demands of such frames with different degrees of the semi-rigidity under the above types of the earthquake are not widely reported.

In this paper, the seismic behavior of SR connected steel frames is critically examined for both near and far-field earthquakes. In order to make the study a comprehensive one (i) two steel special moment resisting frames (SMRF), namely, a five-storey and a ten-storey, three-bay steel frames having different degrees of semi-rigidity (DSR) are considered; (ii) the responses of the frame are obtained for a suite of 5 earthquakes in each of the three different types of earthquake, namely, the far-field and near-field earthquakes (with forward directivity and fling-step effects); (iii) earthquakes are scaled to three different PGA levels, 0.2 g (low), 0.4 g (medium) and 0.8 g (high); and (iv) a large number of seismic demand parameters consisting of the maximum inter-storey drift ratio (MIDR), peak top floor displacement, maximum base shear, number of plastic hinges, and SRSS of maximum plastic hinge rotations are considered. The connection nonlinearity is considered by providing the backbone curves for the zero-length multilinear plastic link element (Akkar *et al.* 2005), and material nonlinearity defined by the default plastic hinge property using the general-purpose software SAP2000v21 (2019).

2. Theory

Semi-rigid beam-column connection models are basically described by their moment-rotation curves. There are several models in the literature that depict the most probable representation of a moment-rotation curve of the SR connection, namely, the Kishi-Chen Power model, Frye and Morris polynomial model, etc. (Frye and Morris 1975, Kishi and Chen 1990). The SR connection model as implemented in the standard software SAP2000 is adopted here and is described below.

2.1 Semi-rigid connection model and its software implementation

SR connections have the same generic connection model based on (ANSI/AISC-341 (2016)) SMF SR connection shown in Fig. 2. On the generic plot, for all connections, 'M_{yc}' is the yield moment capacity of the connection which is taken as the two-third of the plastic moment capacity of connection 'M_{pc}.' The flexural resistance of the connection (M_p) is taken as 80% of M_{pc}. The flexibility of the SR connection depends on the connection stiffness parameter α, i.e., $R_{ki} = \alpha\ (EI_{beam}/L_{beam})$, where R_{ki} is the initial connection stiffness and strength parameter β, i.e., the ratio of the M_{pc} to the plastic moment capacity of the connected beam 'M_{pb}.' Chan and Chui (2000) suggested that the story drift angle should be greater than 0.04 radian, i.e., $\theta_u \geq 0.04$ radian. Thus, the rotation (θ_{pc}) considered at the ultimate resistance or peak moment of the connection is taken as 80% of θ_u as shown in Fig. 2. Linear continuation of the strength loss beyond 80% leads to a maximum rotation of 0.072 radian at which the connection strength reduces to zero. Two joint zero-length multilinear plastic link elements with rotational nonlinearity in R3 direction are used to model the semi-rigid connection in the general-purpose software SAP2000. The kinematic hysteretic behavior model is selected in the SAP2000 for the SR connection to consider the energy dissipation in connections. The two joint zero-length link elements are provided at the beam ends only, and the SR connected structure model is shown in Fig. 3.

Various researchers proposed various hysteresis models for the connection and material nonlinearity; both are located in the joints or at the ends of the member (Kitipomchai *et al.* 1990, Liu *et al.* 2008). The important nonlinearities associated with the SR steel frame may be classified into three categories, i.e., connection, geometric and material nonlinearities. The connection nonlinearity includes the primary distortion of the beam-column steel connection in the form of rotational deformation, θ, due to the in-plane bending moment as well as the drift (P-Δ effect) of the frame. To capture the probable inelastic deformation, the beam member is modeled like an elastic member with flexural M3 plastic hinges at the ends and P-M3 flexural hinges employed in the column ends. The hysteresis curve for the default plastic hinge as per ASCE-41 (2017) is shown in Fig. 4. The default hinges are provided at the ends of the beam and column faces at an absolute distance of 0.05 of the length. The default hinges of nature P-M3 type (axial force with coupled bending moment hinges considering the interaction of bending moment and axial force) for columns and M3 type (moment hinges) for beams are selected.

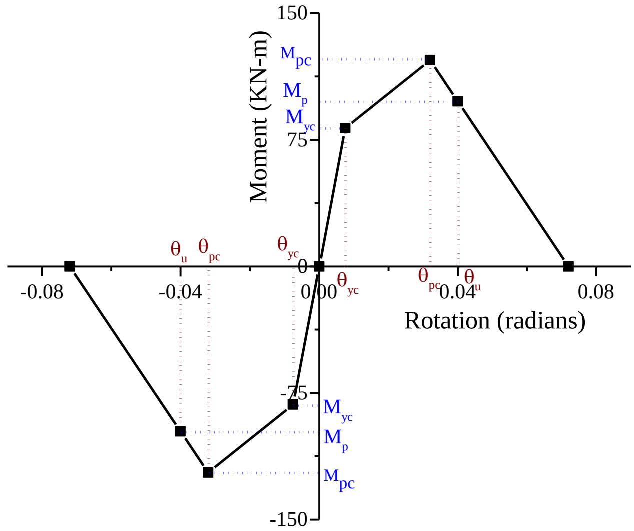

Fig. 2 Typical moment-rotation backbone curve for the semi-rigid connection

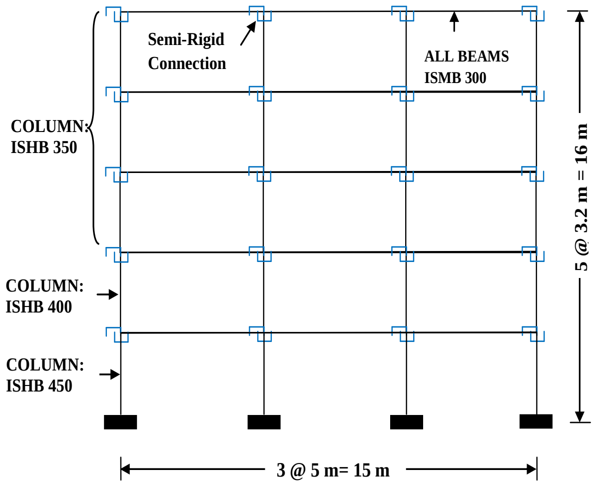

Fig. 3 A 5-Storey semi-rigid connected steel frame

Table 1 Details of section sizes for steel frames

Steel Frame	Story/ Floor	Beam Section	Column Section	Story Height	Bay Width	fy* (N/mm2)	E# (N/mm^2)	Poisson ratio
Rigid Frame								
10-Story Steel Frame (A0)	1st- 6th	W 14 X 38	W 14 X 68	3.2 m	5 m	250	2.10E+05	0.3
	7th-10th	W 14 X 38	W 14 X 53	3.2 m	5 m	250	2.10E+05	0.3
5-Story Steel Frame (B0)	1st	ISMB 300	ISHB 450	3.2 m	5 m	250	2.10E+05	0.3
	2nd	ISMB 300	ISHB 400	3.2 m	5 m	250	2.10E+05	0.3
	3rd- 5th	ISMB 300	ISHB 350	3.2 m	5 m	250	2.10E+05	0.3
Semi-rigid Frame (α=10, β=1.5)								
Steel Frame	Story/ Floor	Beam Section	Column Section	Story Height	Bay Width	(N/mm2)	E (N/mm^2)	Poisson ratio
10-Story Steel Frame(A8)	1st- 6th	W 12 X 35	W 14 X 68	3.2 m	5 m	250	2.10E+05	0.3
	7th-10th	W 12 X 35	W 14 X 53	3.2 m	5 m	250	2.10E+05	0.3
5-Story Steel Frame(B8)	1st	ISHB 225	ISHB 450	3.2 m	5 m	250	2.10E+05	0.3
	2nd	ISHB 225	ISHB 400	3.2 m	5 m	250	2.10E+05	0.3
	3rd- 5th	ISHB 225	ISHB 350	3.2 m	5 m	250	2.10E+05	0.3

*fy: Steel Grade; #E : Modulus of Elasticity

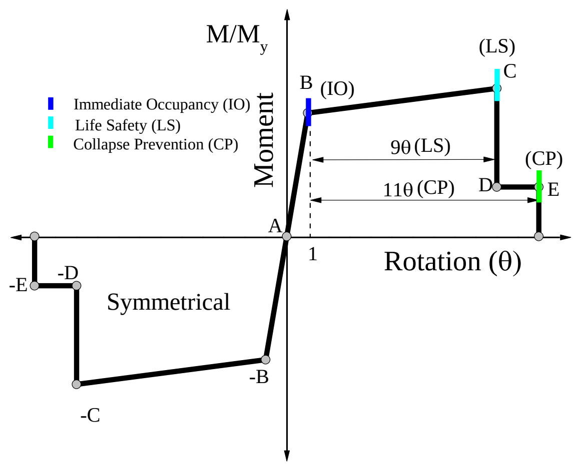

Fig. 4 Backbone curve of ASCE 41-17 default plastic hinge and acceptance criteria (IO, LS, CP)

The acceptance criteria values defined in Table 9.6 of ASCE 41 are directly used for default hinges in SAP2000. In the backbone curve, three performance levels of hinges are defined, namely, IO (Immediate Occupancy), LS (Life Safety) and CP (Collapse Prevention).

Furthermore, each SR connection is modeled as a separate multilinear plastic link element at the beam ends and depicted in the generic plot in Fig. 3.

2.2 Analysis

The nonlinear time-history analysis (NTHA) for different time histories of ground motion is performed in the SAP2000. In the SAP2000, the direct integration scheme is adopted; Rayleigh proportional damping is used considering the 5% damping for the first and second vibration modes for all cases. Hilber-Hughes-Taylor direct integration scheme is employed for the integration. The required inputs for modeling the semi-rigid connection as per the SAP2000 are provided.

3. Numerical study

For the numerical study, two rigid frames with ten and five stories are designed based on the Indian Standard criteria (IS-800 2007). The sections are designed to resist gravity loads as well as seismic loads (IS-875 1987; IS-1893 2016). Designed members and cross-sections are shown in Table 1. For the design, a 150 mm deep concrete deck is provided over the beams including the floor finish, and 225 mm thick brick masonry partition walls are provided. The effective uniformly distributed floor dead load on the beams, roof dead load and live load are taken as 20KN/m, 15KN/m, and 4KN/m respectively (see Fig. 5). The design is based on the strong column-weak beam (SCWB) concept. The ratio of the plastic moment capacity of the column to the plastic moment capacity of the beam is more than 1.2 as per the requirement in the SCWB. The panel zone has been provided with continuity and doubler plates for the capacity enhancement so that it remains elastic. The connection details and their designations are shown in Table 2.

For semi-rigid frames, different degrees of semi-rigidity (DSR) are incorporated by assigning suitable values of the two parameters α and β (defined in section 2.1). A higher value of α denotes a higher rigidity of the connection and vice versa. Similarly, a higher value of β indicates a higher strength ratio of the connection and vice versa. The sizes of the beams and columns of the semi-rigid frames are designed using three values of α (3, 10, 22) and β (0.75, 1.1, 1.5). Note that α modifies beam sizes, and β modifies the

Table 2 Categorization of the beam-column connection

Frame	Frame ID	β (Strength Parameter)	α (Stiffness Parameter)	Frame	Frame ID	β (Strength Parameter)	α (Stiffness Parameter)
5-Storey 3-Bay SMF Frame	B0 (Rigid)	Centerline Model		10-Storey 3-Bay SMF Frame	A0 (Rigid)	Centerline Model	
	B1 (SR)	0.75	3		A1 (SR)	0.75	3
	B2 (SR)		10		A2 (SR)		10
	B3 (SR)		22		A3 (SR)		22
	B4 (SR)	1.1	3		A4 (SR)	1.1	3
	B5 (SR)		10		A5 (SR)		10
	B6 (SR)		22		A6 (SR)		22
	B7 (SR)	1.5	3		A7 (SR)	1.5	3
	B8 (SR)		10		A8 (SR)		10
	B9 (SR)		22		A9 (SR)		22

Table 3 Sample inputs for modeling semi-rigid connections in SAP2000

Building	Frame ID	R_{ki}	Damping	M_{yc} (KN-m)	M_{pc} (KN-m)	M_p KN-m)	θ_{yc} (rad)	θ_p (rad)	θ_u (rad)
10-Story	A8 (α=10, β=1.5)	67284	0.05	253.26	378	321.25	0.00376	0.032	0.04
5-Story	B8 (α=10, β=1.5)	36136	0.05	163.74	244.4	195.51	0.00453	0.032	0.04

ratio between plastic moment capacities of connection and beam. The corresponding section sizes of the semi-rigid frame for a particular combination of α (=10) and β (=1.5) are also shown in Table 1.

Typical input information to be provided in SAP2000 for analyzing the semi-rigid frame is shown in Table 3. The first three natural frequencies of the investigated rigid and semi-rigid frames are shown in Table 4. The three different types of scaled ground motions are considered with three different levels of PGA, i.e., 0.2 g, 0.4 g, and 0.8 g. The elastic response spectra with mean spectra for far-field, near-field with directivity and fling-step effect earthquakes are shown in Figs. 5(b)-5(d). The far-field ground motion records are chosen from the (FEMA-P695 (2009)) report, and the near-field record selection is based on Joyner Boore distance (R_{jb} < 15 km). The details of ground motion records are given in Table 5.

Table 4 The first three natural frequencies of rigid and semi-rigid frames

Sr. No	10-Story Frame				5-Story Frame			
	DSR (α)	Natural Frequency (Hertz)			DSR (α)	Natural Frequency (Hertz)		
		f1	f2	f3		f1	f2	f3
1	3	0.693	2.421	5.116	3	0.375	1.194	2.207
2	10	0.84	2.8	5.52	10	0.47	1.455	2.613
3	22	0.9	2.96	5.69	22	0.508	1.558	2.775
4	Rigid	0.967	3.133	5.885	Rigid	0.548	1.668	2.951

Table 5 Ground motion records*

No.	Event Year	Ground Motion-Component	M_w	PGA (g)	PGV (cm/s)	PGD (cm)	R_{jb} (km)
Far-field earthquake (FF)							
1	1995	Kobe-Nishi-000	6.9	0.51	37.28	9.53	25.2
2	1992	Landers-TR	7.3	0.42	42.35	13.84	19.74
3	1978	Tabas-Ferdows-L	7.4	0.093	5.4	2.24	89.76
4	1987	Superstition hill-POE-270	6.5	0.45	35.72	8.81	22.25
5	1971	San Fernando-90	6.6	0.21	18.87	12.42	124.38
Near-field with directivity effect (NFD)							
1	1992	Erzincan-EW	6.7	0.5	64.32	21.91	0.1
2	1994	Northridge-Sylmar-018	6.7	0.83	117.5	34.45	1.74
3	1979	Imperial Valley-270	6.53	0.35	75.58	57.15	7.87
4	1992	Cape Mendocino-90	7	0.66	89.68	29	0.1
5	1999	Kocaeli-Duzce-180	7.4	0.31	58.86	44.06	13.6
Near-field with fling-step effect (NFF)							
1	1999	Chi-Chi-TCU072-EW	7.6	0.46	83.60	209.67	7.9
2	1999	Chi-Chi-TCU065-EW	7.6	0.76	128.32	228.41	2.5
3	1999	Kocaeli-Sakarya-EW	7.4	0.41	82.05	205.93	7.9
4	1999	Chi-Chi-TCU076-EW	7.6	0.33	65.93	101.65	3.2
5	1999	Chi-Chi-TCU084-EW	7.6	0.98	140.43	204.59	11.4

*Mw: Magnitude; R_{jb}: Closest Distance

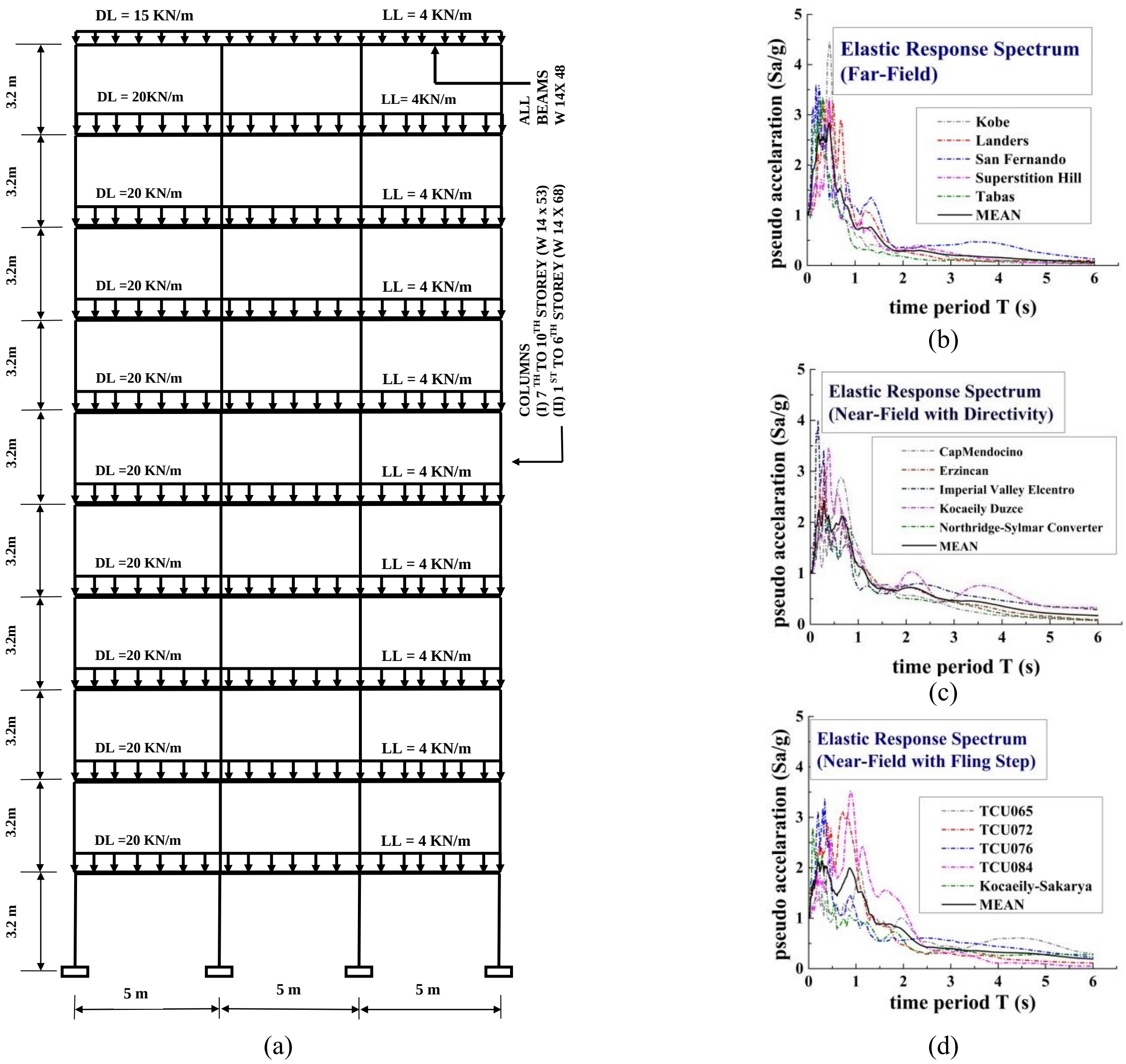

Fig. **5** (a) A 10-story rigid frame with loading, and (b)-(d) elastic response spectra for earthquakes

4. Results and discussion

For the three types of earthquakes, i.e., far-field (FF), near-field with directivity (NFD) and fling-step effects (NFF), the responses are shown in terms of the mean peak and maximum peak values of the five responses obtained from the five-time history records of earthquakes, in each ensemble, for a scaled PGA value. The mean peak value refers to the mean of the peak responses obtained from the ensemble of earthquakes in each type (FF, NFD, and NFF). On the other hand, the maximum peak value refers to the maximum absolute peak response obtained from the entire ensemble of earthquakes in each type. For illustration, the plots of the mean peak and maximum peak floor displacements and MIDRs are shown in Figs. 6 and 7 for two degrees of semi-rigidity (DSR) represented by (α=10; β=1.5) and (α=3; β=0.75). In the figures, it is observed that there are six plots in each figure. Three plots represented by the firm lines correspond to the ensemble mean peak values, whereas the dotted lines indicate the maximum of the peak values obtained from the ensemble. It is seen from Fig. 6 that the patterns of the variation of the mean peak floor displacement and maximum peak floor displacement along the height are not exactly of the same type. There are some differences between the two shapes. Further, the mean peak values are significantly less than the maximum peak values of floors, especially at the top floor level. The pattern of the variation of the peak floor displacement along the height also varies mildly with the type of earthquake and PGA value.

On the other hand, the patterns of variation of the MIDR along the height of the building remain almost the same for the three PGA values and the three types of the earthquake. However, like the case of floor displacement, the mean peak values of the MIDR are much less than the maximum peak values of the MIDR. Further, it is observed that both for the 5-story and 10-story frames, the maximum values of the MIDR occur at the third-floor level.

4.1 Effect of the degree of semi-rigidity on the mean peak top floor displacement

The effect of the degree of semi-rigidity (DSR) on the five response quantities of interest is shown in Figs. 8-11,

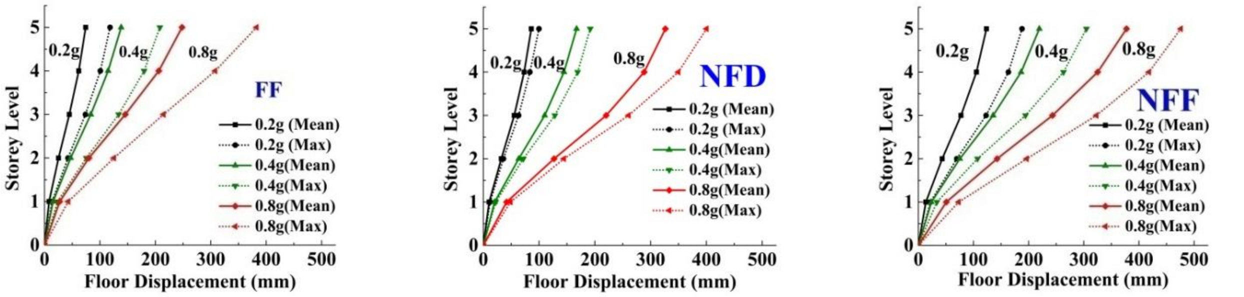

(a) 5-story SR frame at DSR (α=10; β=1.5)

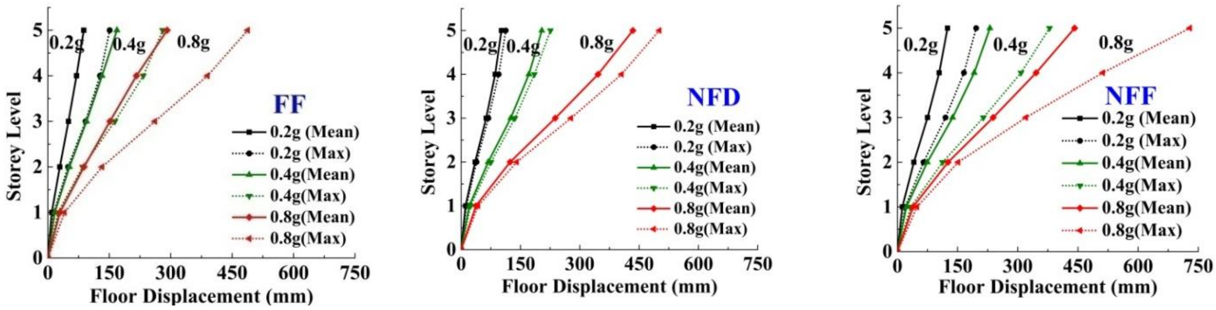

(b) 5-story SR frame at DSR (α=3; β=0.75)

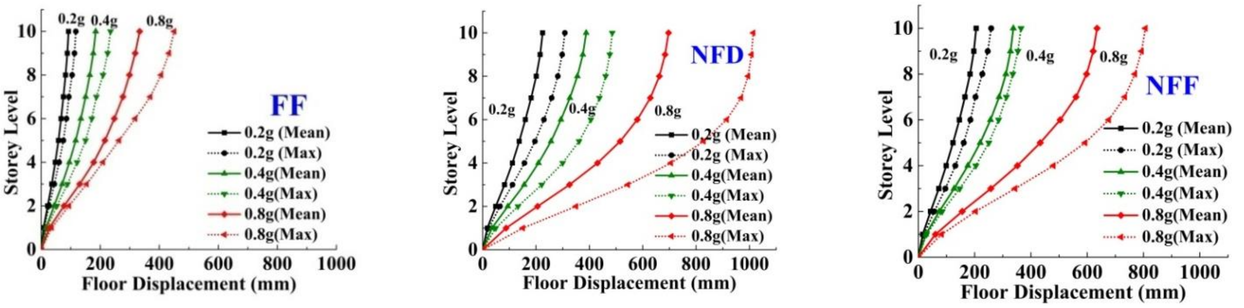

(c) 10-story SR frame at DSR (α=10; β=1.5)

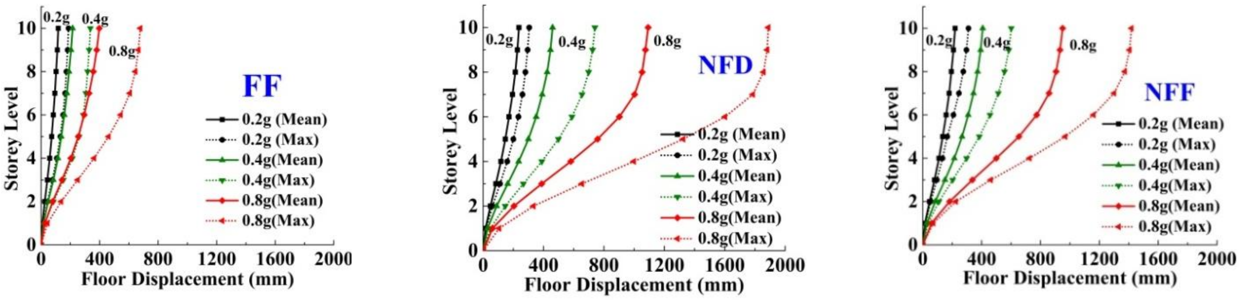

(d)10-story SR frame at DSR (α=3; β=0.75)

Fig. 6 Variations of the peak floor displacements for different earthquakes at three PGA levels

and Tables 6-9. Figs. 8 and 9 show the variations of the mean peak top floor displacements for different earthquakes at the three PGA values for the set of DSR (β=0.75 and 1.5), shown in Table 2. Note that α=3 and α=22 denote highly flexible joint (high degree of semi-rigidity) and less flexible joint (low degree of the semi-rigidity) respectively. It is seen from Figs. 8 and 9 that for the 5-story frame, as the DSR decreases, the mean peak top floor displacement also decreases as it would be expected. Further, it is observed that the near-field earthquake with the fling-step effect provides more value of the mean peak top floor displacement as compared to the far-field earthquake for all the three values of the PGA. The difference in the two values increases with the increase in the value of the PGA.

The same observations hold true for the 10-story frame with the following changes: (i) at the high value of the PGA (0.8g), the change in the mean peak top floor displacement with the change in the DSR from α=3 to 10 is significantly more as compared to the 5-story frame and (ii) the NFD earthquakes produce more value of the mean peak top floor displacement. Note that for the rigid frame, both NFD and NFF earthquakes provide nearly the same mean peak top floor displacement.

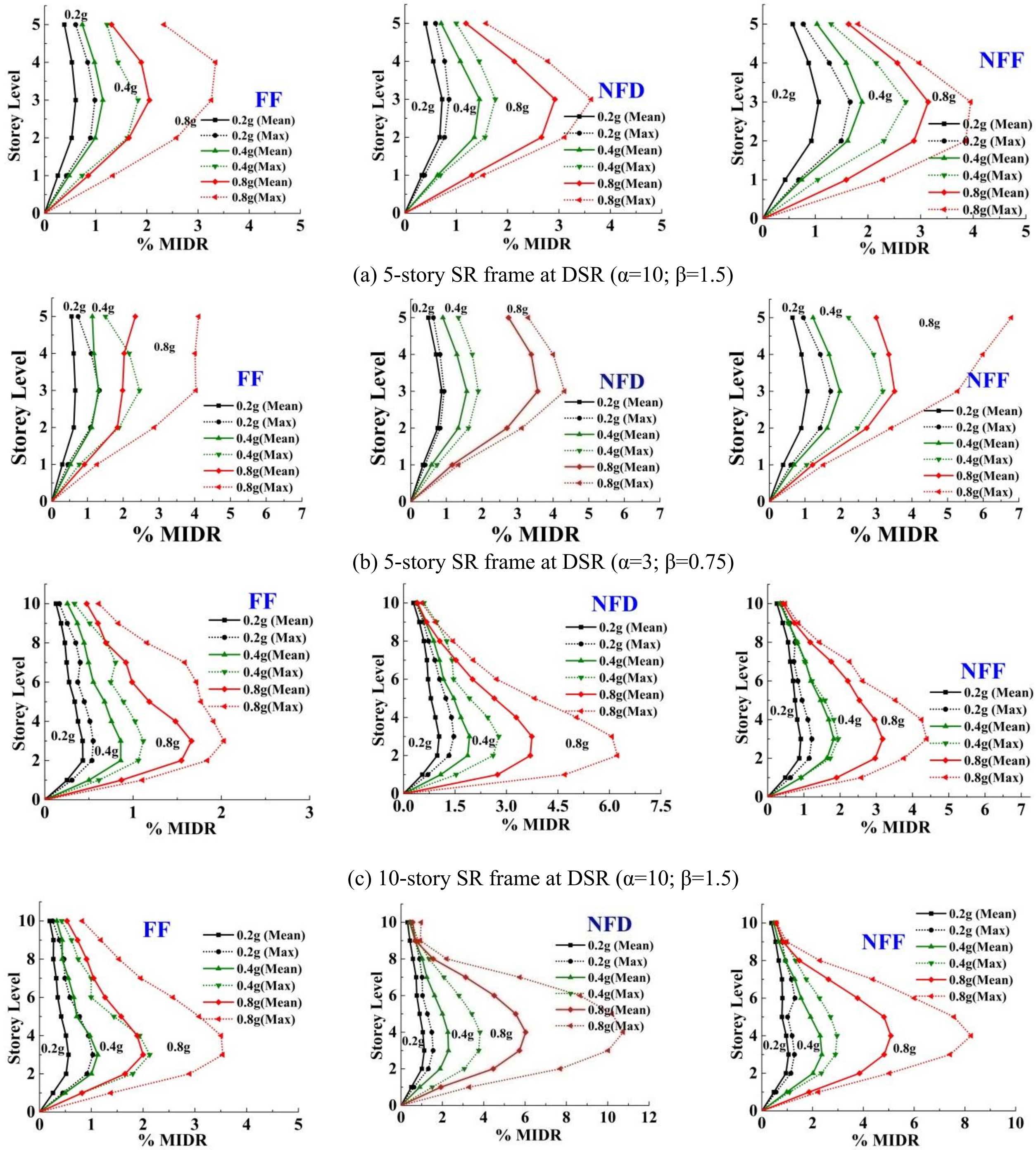

(a) 5-story SR frame at DSR (α=10; β=1.5)

(b) 5-story SR frame at DSR (α=3; β=0.75)

(c) 10-story SR frame at DSR (α=10; β=1.5)

(d) 10-story SR frame at DSR (α=3; β=0.75)

Fig. 7 Variations of the MIDR for different earthquakes at three PGA levels

4.2 Effect of the degree of semi-rigidity on MIDR

Figs. 10 and 11 show the effect of the DSR on the MIDR. The effect of the DSR on the MIDR is nearly the same as that observed for the mean peak top floor displacement for both five and ten-story frames.

4.3 Effect of the degree of semi-rigidity on the mean peak base shear

Tables 6 and **7** show the effect of the DSR on the mean peak base shear for the three different earthquakes at the three PGA values for the 5- and 10-story frames. The values in the tables are normalized values, i.e., the ratio between the mean peak value of the base shear to that of the rigid

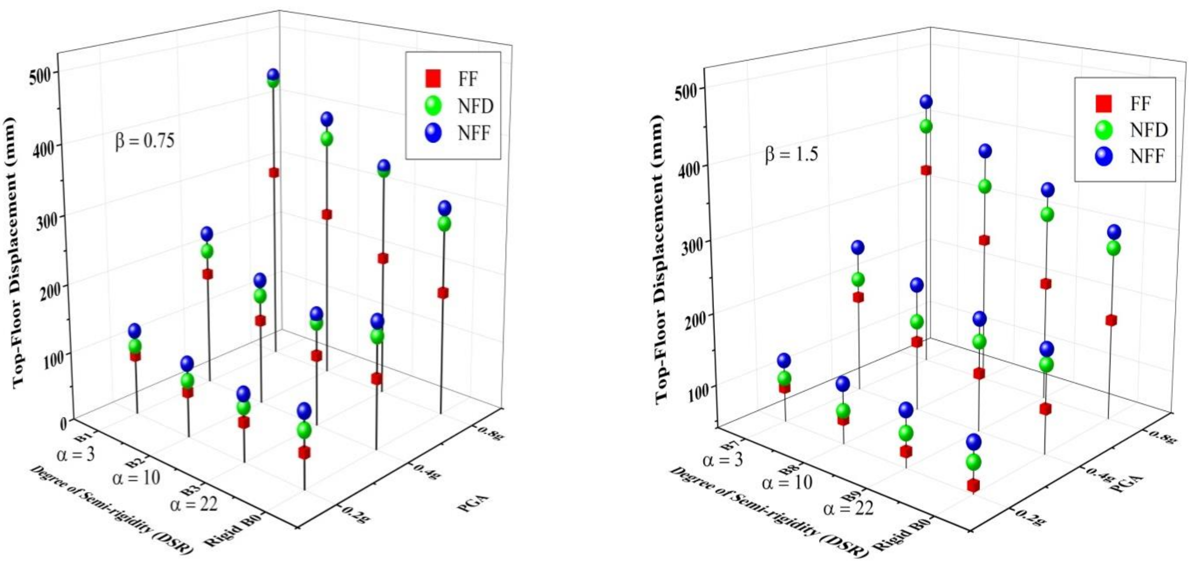

(a) β=0.75 (b) β=1.5

Fig. 8 Mean peak top floor displacement for different earthquakes at three PGA levels and three α values for the five-story frame (a)-(b)

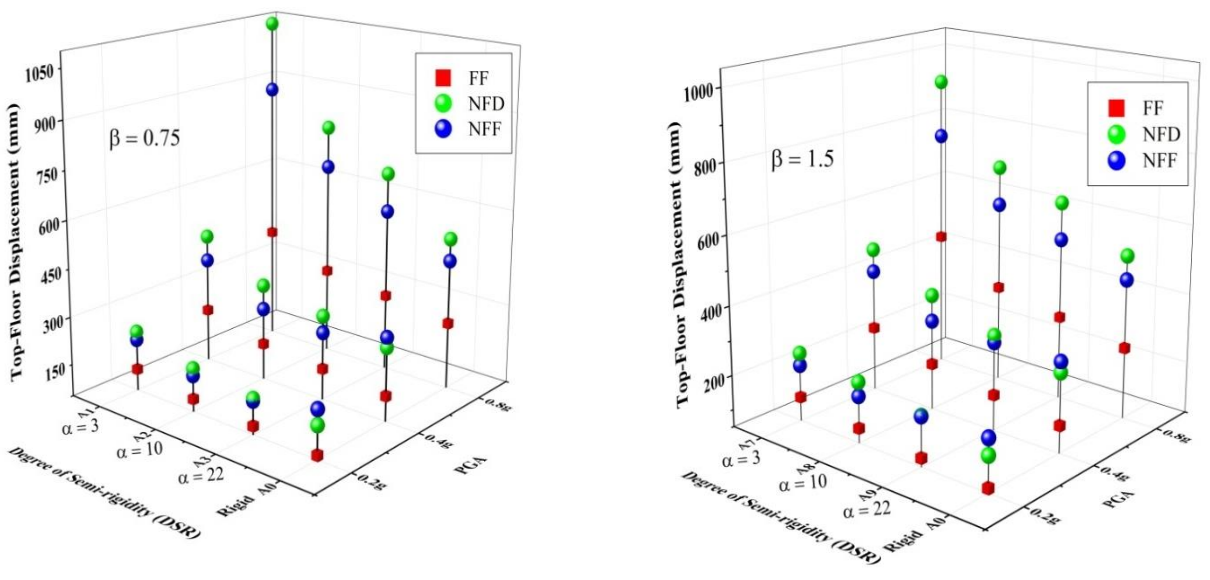

(a) β=0.75 (b) β=1.5

Fig. 9 Mean peak top Floor displacement for different earthquakes at three PGA levels and three α values for the ten-story frame (a)-(b)

frame. It is seen from the tables that for the low value of the PGA (0.2 g), it is generally observed that the base shear increases as the value of α increases for the near field earthquakes, as it would be expected. This change is pronounced for the NFF. For the far-field earthquake, the DSR does not practically influence the base shear. This is the case because, for the low value of the PGA, the frame remains in the elastic state. As a consequence, the link elements do not significantly change the lateral stiffness of the frame resulting in practically no change in the base shear for small lateral displacements of the frame at the low value of the PGA.

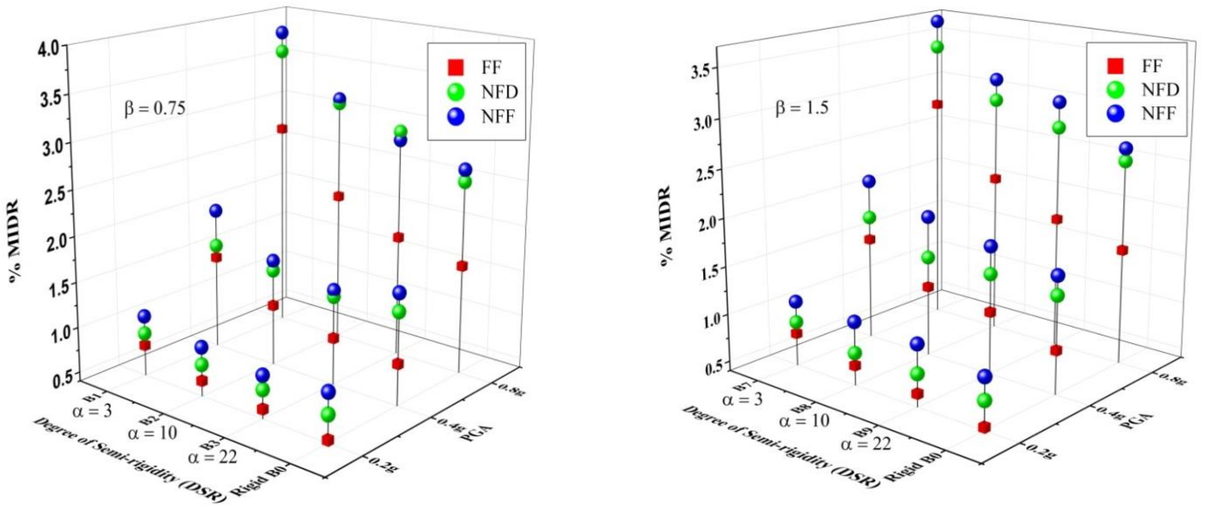

(a) β=0.75 (b) β=1.5

Fig. 10 Mean peak MIDR for different earthquakes at three PGA levels and three α values for the five-story frame (a)-(b)

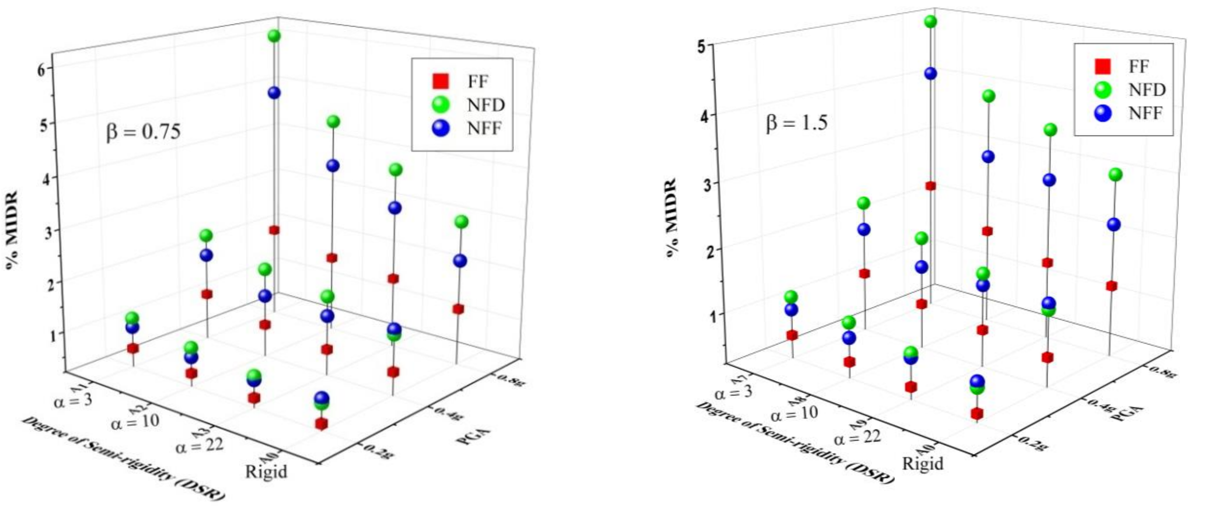

(a) β=0.75 **(b)** β=1.5

Fig. 11 Mean peak MIDR for different earthquakes at three PGA levels and three α values for the ten-story frame (a)-(b)

However, for the relatively large displacement, as it is caused by the near field earthquake even at the low value of the PGA, noticeable change in the base shear is observed even due to the small change in the lateral stiffness of the frame. For higher values of the PGA, namely, 0.4g and 0.8g, no consistent pattern emerges. For most of the cases, no significant change in the base shear is seen with the change in the DSR. This happens due to the inelastic excursion of the semi-rigid frame at higher values of the PGA leading to the development of the base shear which does not show any consistent pattern due to the complex mechanism of seismic energy dissipation in the frame.

4.4 Effect of the degree of semi-rigidity on the number of plastic hinges and SRSS of plastic hinge rotations

The effect of the DSR on the extent of plastification denoted by the number of plastic hinges formed and the SRSS of maximum plastic hinge rotations is shown in Tables 8 and 9. It is seen from the tables that for the far-field earthquake, the extent of plastification is marginal at the PGA value of 0.4g for both frames with semi-rigid and rigid connections. However, at the PGA value of 0.8 g, considerable plastification in terms of the number of plastic

Table 6 Mean peak base shear (normalized) for different earthquakes for the 5-story frame

DSR		Frame ID	FF			NFD			NFF		
β	α		0.2 g	0.4 g	0.8 g	0.2 g	0.4 g	0.8 g	0.2 g	0.4 g	0.8 g
0.75	3	B1	0.95	0.87	0.84	0.82	0.74	0.74	0.58	0.63	0.65
	10	B2	0.96	0.82	0.79	0.83	0.70	0.70	0.68	0.66	0.66
	22	B3	0.98	0.75	0.75	0.84	0.70	0.71	0.70	0.65	0.69
1.1	3	B4	0.99	0.95	0.94	0.82	0.84	0.82	0.61	0.68	0.80
	10	B5	1.00	0.92	0.89	0.93	0.82	0.80	0.80	0.78	0.79
	22	B6	0.99	0.85	0.83	0.95	0.83	0.81	0.86	0.78	0.79
1.5	3	B7	0.96	0.98	1.00	0.82	0.85	0.93	0.56	0.71	0.84
	10	B8	0.97	0.98	0.99	0.93	0.92	0.90	0.85	0.87	0.89
	22	B9	1.00	0.94	0.91	1.00	0.93	0.90	0.96	0.91	0.87
Maximum			1.00	0.98	1.00	1.00	0.93	0.93	0.96	0.91	0.89
Minimum			0.95	0.75	0.75	0.82	0.70	0.70	0.56	0.63	0.65
Absolute % Difference			5	25	25.5	18	31.3	30	44	36.8	35.1

Table 7 Mean peak base shear (normalized) for different earthquakes for the 10-story frame

DSR		Frame ID	FF			NFD			NFF		
β	α		0.2 g	0.4 g	0.8 g	0.2 g	0.4 g	0.8 g	0.2 g	0.4 g	0.8 g
0.75	3	A1	0.82	0.73	0.65	0.64	0.52	0.51	0.58	0.60	0.65
	10	A2	0.98	0.85	0.72	0.73	0.56	0.56	0.61	0.55	0.64
	22	A3	0.99	0.90	0.75	0.75	0.60	0.62	0.64	0.58	0.67
1.1	3	A4	0.82	0.79	0.70	0.69	0.63	0.59	0.60	0.67	0.78
	10	A5	0.97	0.98	0.83	0.89	0.70	0.67	0.70	0.67	0.72
	22	A6	0.98	0.99	0.87	0.92	0.75	0.73	0.74	0.69	0.76
1.5	3	A7	0.82	0.82	0.77	0.70	0.72	0.74	0.60	0.71	0.90
	10	A8	0.93	0.97	0.92	0.96	0.85	0.77	0.75	0.77	0.82
	22	A9	0.99	1.00	0.98	1.00	0.87	0.82	0.81	0.79	0.86
Maximum			0.99	1.00	0.98	1.00	0.87	0.82	0.81	0.79	0.90
Minimum			0.82	0.73	0.65	0.64	0.52	0.51	0.58	0.55	0.64
Absolute % Difference			18	27	35	36	48	49	42	45	36

hinges and the SRSS of plastic hinge rotations is observed for all types of earthquakes. For the near field earthquake, the plastification is more as compared to the far-field earthquake. Further, it is seen that for the higher value of β (1.5), both the number of plastic hinges and SRSS of plastic hinge rotations are more as compared to the lower values of β. This clearly shows the relative effect of the parameter β on the extent of plastification. Even for the less value of α (3), both the number of plastic hinges and SRSS of plastic hinge rotations are increased considerably when the value of β is increased to 1.5. This means that for a much weaker beam (compared to the column), comparable seismic energy is dissipated in the plastification of beams as compared to that dissipated in the connection link elements (having very less connection stiffness) at the high value of the PGA (0.8g). For a relatively low value of the PGA (0.4 g which is the specified extreme level earthquake in many codes), most of the seismic energy is dissipated in the link elements without allowing the weaker beams to undergo large inelastic excursion. Thus, for a moderately strong earthquake, a semi-rigid frame having a much weaker beam (and with less α value) may prove to be beneficial in protecting beams against seismic damage.

4.5 Energy dissipation in SR frames

The energy dissipated in SR frames is due to the modal energy and link hysteretic energy dissipation. The latter also accounts for the energy dissipation in the plastic hinges formed close to the plastic links of the SR model. Table 10 shows the energy dissipated in two SR frames with different DSR. It may be seen from the table that for the higher value of α (=10), a higher percentage of input energy is dissipated in the form of hysteretic energy as compared to the lower

Table 8 Total number of plastic hinges formed for different earthquakes for both 5- and 10-story frames

DSR		Frame ID	FF		NFD		NFF		Frame ID	FF		NFD		NFF	
β	α		0.4 g	0.8 g	0.4 g	0.8 g	0.4 g	0.8 g		0.4 g	0.8 g	0.4 g	0.8 g	0.4 g	0.8 g
0.75	3	B1	0	4	0	6	0	6	A1	0	2	2	8	2	9
	10	B2	0	1	0	5	0	5	A2	0	2	2	7	1	5
	22	B3	0	1	0	5	0	4	A3	0	2	2	5	0	5
1.1	3	B4	0	5	0	7	1	7	A4	1	4	4	7	2	6
	10	B5	0	3	0	6	1	6	A5	0	2	3	9	1	6
	22	B6	0	2	0	5	1	5	A6	0	2	2	18	1	7
1.5	3	B7	1	12	1	13	1	15	A7	1	7	4	39	3	15
	10	B8	0	9	0	14	2	20	A8	0	6	8	41	3	27
	22	B9	0	8	0	22	3	22	A9	0	10	7	44	4	38
Rigid		B0	4	21	12	33	21	33	A0	0	30	33	61	37	57

Table 9 SRSS of maximum plastic hinge rotations (X 10-3 radians) for different earthquakes for the 5- and 10-story frames

DSR		Frame ID	FF		NFD		NFF		Frame ID	FF		NFD		NFF	
β	α		0.4 g	0.8 g	0.4 g	0.8 g	0.4 g	0.8 g		0.4 g	0.8 g	0.4 g	0.8 g	0.4 g	0.8 g
0.75	3	B1	0.0	1.8	0.0	4.7	0.5	6.4	A1	0.1	1.4	2.2	16.9	0.8	17.4
	10	B2	0.0	0.4	0.0	3.8	0.0	4.9	A2	0.0	0.9	1.4	14.8	0.0	11.6
	22	B3	0.0	0.2	0.0	4.0	0.0	4.7	A3	0.0	0.6	0.9	19.6	0.0	10.2
1.1	3	B4	0.2	4.3	0.0	6.8	1.7	11.1	A4	0.3	3.8	2.7	17.2	0.6	18
	10	B5	0.0	1.2	0.0	4.6	0.1	9.1	A5	0.0	1.3	3.1	25.8	0.1	14.6
	22	B6	0.0	0.8	0.0	5.6	0.1	7.4	A6	0.0	0.7	1.9	27.4	0.2	11.4
1.5	3	B7	0.5	7.2	0.1	9.6	1.9	15.5	A7	0.4	5.9	4.2	35.1	2.5	22.1
	10	B8	0.0	3.1	0.0	8.4	0.9	16.8	A8	0.0	2.6	4.7	34.2	1.1	17.8
	22	B9	0.0	2.3	0.0	9.2	1.0	14.1	A9	0.0	1.6	3.8	36.1	1.3	18.3
Rigid		B0	2.3	25.1	12.7	55.3	23.5	61.1	A0	0.0	10.8	12.3	84.2	17.4	58.3

value of α (=3). The latter case corresponds to the more flexible joints (higher degree of semi-rigidity). This is the case because less plastification takes place for the higher degree of semi-rigidity.

4.6 Comparison of responses between the semi-rigid and fully rigid frames

In order to show the explicit difference between the behaviors of semi-rigid and rigid frames, two cases of semi-rigidity denoted by (α=10; β=1.5) and (α=3; β=0.75) are selected. For the above values of the DSR, the mean peak and maximum peak normalized value of the top floor displacement, MIDR, and base shear are shown in Tables 11-13 for three types of earthquakes. The normalization is done with respect to the corresponding values for the rigid frame. It is seen from the tables that the normalized values (ratio) vary depending upon the seismic demand parameter, type of earthquake, value of the PGA and height of the frame. For the maximum peak top floor displacement, MIDR and maximum base shear the ratios vary between 1 to 1.8, 0.96 to 1.68 and 0.75 to 1 respectively for the frame with DSR (α=10; β=1.5). For the frame with DSR (α=3; β=0.75), the corresponding ratios vary between 1.1 to 2.5, 1.11 to 2.99, and 0.51 to 0.96. Thus, it is observed that the variation of the ratios is more for DSR (α=3; β=0.75). Further, the ratios for the base shear confirm that the base shear for the semi-rigid frame is always less than that of the rigid frame. The comparison of the maximum values with the mean values in the tables shows that the scatter of the values in the ensemble varies from 30 to 50%. This scatter is expected to narrow down if the sample size in the ensemble were increased. In most cases, no consistent pattern of the variation with DSR emerges because of the averaging effect.

5. Conclusions

A comprehensive study on the seismic behavior of steel frames with semi-rigid connections is carried out under a number of important parametric variations, namely, the

Table 10 Energy dissipation in SR frames

Frame ID	Earthquake Type_Event Name_PGA	Energy (KN-m)		
		Input Energy	Modal Damping Energy (% Input Energy)	Link Hysteretic Energy (% Input Energy)
10-story SR frame				
A7 (α=3; β=1.5)	FF_Kobe_0.4g	119.61	97.7 (81.69)	0.00 (0.00)
	FF_Kobe_0.8g	447.81	384.02 (85.75)	6.36 (1.42)
	NFD_Kocaeli Duzce_0.4 g	230.50	180.03 (78.1)	6.75 (2.93)
	NFD_Kocaeli Duzce_0.8 g	1456.86	767.76 (52.7)	635.61 (43.63)
	NFF_Chi-Chi TCU065_0.4 g	314.68	297.02 (94.39)	4.69 (1.5)
	NFF_Chi-Chi TCU065_0.8 g	1542.67	1018.12 (66)	500.63 (32.45)
A8 (α=10; β=1.5)	FF_Kobe_0.4 g	168.93	158.08 (93.6)	0.017 (0.01)
	FF_Kobe_0.8 g	602.11	428.94 (71.2)	156.87 (26.05)
	NFD_Kocaeli Duzce_0.4 g	471.47	221.85 (47)	191.42 (40.6)
	NFD_Kocaeli Duzce_0.8 g	1634.59	763.90 (46.7)	850.55 (52.03)
	NFF_Chi-Chi TCU065_0.4 g	568.57	393.59 (69.22)	162.34 (28.55)
	NFF_Chi-Chi TCU065_0.8 g	1740.81	851.73 (48.93)	870.42 (50)
5-story SR frame				
B7 (α=3; β=1.5)	FF_Kobe_0.4 g	60.20	55.94 (92.9)	0.00 (0.00)
	FF_Kobe_0.8 g	232.13	220.14 (94.8)	4.96 (2.14)
	NFD_Kocaeli Duzce_0.4 g	95.04	76.23 (80.21)	0.23 (0.25)
	NFD_Kocaeli Duzce_0.8 g	362.70	238.82 (65.84)	87.33 (24.08)
	NFF_Chi-Chi TCU065_0.4 g	235.60	231.38 (98.21)	0.68 (0.29)
	NFF_Chi-Chi TCU065_0.8 g	989.39	766.95 (77.52)	217.88 (22.02)
B8 (α=10; β=1.5)	FF_Kobe_0.4 g	37.6357	35.08 (93.2)	0.00 (0.00)
	FF_Kobe_0.8 g	145.4097	135.89 (93.5)	6.18 (4.25)
	NFD_Kocaeli Duzce_0.4 g	83.2325	61.34 (73.69)	8.15 (9.8)
	NFD_Kocaeli Duzce_0.8 g	307.523	175.35 (57.02)	123.6 (40.19)
	NFF_Chi-Chi TCU065_0.4 g	309.6809	241.63 (78.03)	58.09 (18.8)
	NFF_Chi-Chi TCU065_0.8 g	1077.7417	603.44 (56)	469.99 (43.61)

Table 11 Normalized peak top floor displacement for 5/10-story frames

FF		NFD		NFF	
Max	Mean	Max	Mean	Max	Mean
5/10-story frame at α= 10 and β= 1.5					
1.4/1.4	1.4/1.5	1.0/1.8	1.0/1.5	1.4/0.9	1.1/0.9
1.3/1.4	1.3/1.4	1.0/1.5	1.0/1.4	1.3/0.9	1.2/1.0
1.5/1.3	1.4/1.3	1.2/1.5	1.2/1.3	1.2/1.4	1.2/1.3
5/10-story frame at α= 3 and β= 0.75					
1.8/2.2	1.7/1.9	1.1/1.8	1.2/1.6	1.4/1.0	1.2/1.1
1.7/2.0	1.6/1.7	1.2/2.3	1.3/1.6	1.7/1.5	1.3/1.2
1.9/2.0	1.6/1.5	1.5/2.8	1.5/2.1	1.9/2.5	1.5/1.9

nature of earthquake, PGA level, degree of semi-rigidity and height of the frame. Three types of earthquakes consisting of the far-field, near-field with directivity and fling step effects are considered.

Each earthquake is scaled to three different levels of PGA, namely, 0.2 g, 0.4 g, and 0.8 g. The degree of semi-rigidity is varied by considering nine different combinations of parameters ‘α’ (stiffness parameter 3,10 and 22) and ‘β’ (strength parameter 0.75,1.1 and 1.5).

Table 12 Normalized peak MIDR for 5/10-story frames

PGA	FF		NFD		NFF	
	Max	Mean	Max	Mean	Max	Mean
5/10-story Frame at α= 10 and β= 1.5						
0.2 g	1.49/1.42	1.43/1.38	0.96/1.68	1.04/0.99	1.37/1.25	1.14/1.17
0.4 g	1.43/1.53	1.35/1.39	0.99/1.66	1.03/1.42	1.33/1.01	1.16/1.2
0.8 g	1.43/1.56	1.30/1.38	1.15/1.48	1.15/1.25	1.12/1.6	1.20/1.32
5/10-story frame at α= 3 and β= 0.75						
0.2 g	2.04/2.66	1.54/1.82	1.05/1.79	1.26/1.12	1.42/1.34	1.15/1.27
0.4 g	1.92/2.92	1.55/1.81	1.06/2.29	1.11/1.69	1.56/1.54	1.22/1.56
0.8 g	1.76/2.4	1.48/1.66	1.37/2.4	1.41/2.01	1.92/2.99	1.34/2.11

Table 13 Normalized maximum base shear for 5/10-story frames

PGA	FF		NFD		NFF	
	Max	Mean	Max	Mean	Max	Mean
5/10-story Frame at α= 10 and β= 1.5						
0.2 g	1.00/1.00	0.974/0.93	1.00/0.998	0.933/0.961	1.00/0.775	0.849/0.747
0.4 g	0.950/0.997	0.985/0.97	0.986/0.834	0.918/0.847	0.861/0.76	0.866/0.769
0.8 g	0.999/0.944	0.990/0.92	0.913/0.752	0.903/0.766	0.910/0.861	0.889/0.823
5/10-story frame at α= 3 and β= 0.75						
0.2 g	0.84/0.97	0.96/0.82	0.84/0.63	0.82/0.64	0.67/0.49	0.58/0.58
0.4 g	0.75/0.85	0.87/0.73	0.72/0.53	0.74/0.52	0.66/0.62	0.63/0.59
0.8 g	0.91/0.68	0.84/0.65	0.75/0.50	0.75/0.51	0.68/0.66	0.65/0.65

The performance of the semi-rigid frames is evaluated with respect to the benchmark responses of the rigid frames. The performance behavior is examined with the help of five seismic demand parameters, namely, the peak top floor displacement, maximum inter-story drift ratio, maximum base shear, total number of plastic hinges, and SRSS of maximum plastic hinge rotations. The conclusions arising out of the numerical study may be summarized as

- At the high value of the PGA, i.e., 0.8 g, the responses (the peak top floor displacement, MIDR, and maximum base shear) are highly sensitive to the variation of the stiffness parameter at the low end (α = 3 to 10); this sensitivity becomes less as the α value is increased. However, for lower values of the PGA (0.2 g and 0.4 g), no such high sensitivity is observed.
- For semi-rigid frames, most of the seismic energy is dissipated in the semi-rigid connections; very less energy is absorbed by way of the formation of plastic hinges for low values of the PGA, ie. 0.2 g and 0.4 g. For the high value of the PGA, there is a sudden increase in the number of plastic hinges in the beams (for β= 1.5), and considerable seismic energy gets dissipated in the plastic hinges formed.
- Semi-rigid frames with relatively weaker beams and less connection stiffness withstand moderately strong earthquake (up to a PGA of 0.4 g) with very less damages in the beams.
- The seismic base shear can be considerably reduced (to the extent of 30% to 45%) by way of providing semi-rigid connections; the reduction achieved is more for the near field earthquakes.
- Beyond a particular value of the stiffness parameter (α=10), the MIDR and peak top story displacement for the semi-rigid frames marginally increases as compared to the rigid frames.
- Large variations in responses in the ensemble, especially for the top floor displacement, MIDR, and base shear are observed for a particular type of earthquake. Therefore, more studies are required to investigate the mean responses either by considering a large number of earthquakes in the ensemble or by removing earthquakes which yield significantly different responses as compared to the other earthquakes in the ensemble.

Emerging out of the conclusions, some recommendations regarding the use of the semi-rigid frame in practical designs could be provided as below:

a. Semi-rigid frames prove to be more beneficial as compared to the rigid frames in seismic prone areas, especially for reduced base shear.

b. The difference in the behaviors of the semi-rigid frame under far-field and near-field earthquakes is not very significant as compared to the rigid frames; therefore, the semi-rigid frames are equally good in both near and far-field earthquakes.

c. For design purposes, a moderate degree of semi-rigidity (like α=10 and β=1.5) is desirable for the effective seismic performance of semi-rigid frames.

References

Abdollahzadeh, G., Faghihmaleki, H. and Esmaili, H. (2016), "Comparing Hysteretic Energy and inter-story drift in steel frames with V-shaped brace under near and far fault earthquakes", *Alexandria Eng. J.,* **57**(1), 301-308. https://doi.org/10.1016/j.aej.2016.09.015.

Akkar, S., Yazgan, U. and Gülkan, P. (2005), "Drift estimates in frame buildings subjected to near-fault ground motions", *J. Struct. Eng.*, **131**(7), 1014-1024. https://doi.org/10.1061/(ASCE)0733-9445(2005)131:7(1014).

Aksoylar, N.D., Elnashai, A.S. and Mahmoud, H. (2011), "The design and seismic performance of low-rise long-span frames with semi-rigid connections", *J. Constr. Steel Res.*, **67**(1), 114-126. https://doi.org/10.1016/j.jcsr.2010.07.001.

Al-Bermani, F., Li, B., Zhu, K. and Kitipornchai, S. (1994), "Cyclic and seismic response of flexibly jointed frames", *Eng. Struct.*, **16**(4), 249-255. https://doi.org/10.1016/0141-0296(94)90064-7.

Alavi, B. and Krawinkler, H. (2004), "Behavior of moment-resisting frame structures subjected to near-fault ground motions", *Earthq. Eng. Struct. D.*, **33**(6), 687-706. https://doi.org/10.1002/eqe.369.

ANSI/AISC-341 (2010), *Seismic provisions for structural steel buildings*, Chicago, Illinois 60601-1802.

ANSI/AISC-341 (2016), *Seismic Provision for Structural Steel Buildings*, American Institute of Steel Construction, Chicago.

Archuleta, R.J. and Hartzell, S.H. (1981), "Effects of fault finiteness on near-source ground motion", *Bull. Seismol. Soc. Am.*, **71**(4), 939-957.

ASCE-41 (2017), *ASCE 41-17: Seismic Evaluation and Retrofit Rehabilitation of Existing Buildings*,

Asgarian, B., Norouzi, A., Alanjari, P. and Mirtaheri, M. (2012), "Evaluation of seismic performance of moment resisting frames considering vertical component of ground motion", *Adv. Struct. Eng.*, **15**(8), 1439-1453. https://doi.org/10.1260/1369-4332.15.8.1439.

Bayat, M. and Zahrai, S.M. (2017), "Seismic performance of mid-rise steel frames with semi-rigid connections having different moment capacity", *Steel Compos. Struct.*, **25**(1), 1-17. https://doi.org/10.12989/scs.2017.25.1.001.

Bertero, V.V., Mahin, S.A. and Herrera, R.A. (1978), "Aseismic design implications of near-fault San Fernando earthquake records", *Earthq. Eng. Struct. D.*, **6**(1), 31-42. https://doi.org/10.1002/eqe.4290060105.

Bray, J.D. and Rodriguez-Marek, A. (2004), "Characterization of forward-directivity ground motions in the near-fault region", *Soil Dynam. Earthq. Eng.*, **24**(11), 815-828. https://doi.org/10.1016/j.soildyn.2004.05.001.

Chan, S.L. and Chui, P.T. (2000), *Non-linear static and cyclic analysis of steel frames with semi-rigid connections*, Science Ltd, Kidlington, Oxford OX5 1GB, UK.

Daryan, A.S., Sadri, M., Saberi, H., Saberi, V. and Moghadas, A.B. (2014), "Behavior of semi-rigid connections and semi-rigid frames", *Struct. Des. Tall Spec. Build.*, **23**(3), 210-238. https://doi.org/10.1002/tal.1032.

Davoodi, M., Sadjadi, M., Goljahani, P. and Kamalian, M. (2012). "Effects of near-field and far-field earthquakes on seismic response of sdof system considering soil structure interaction", *Proceedings of the 15th World Conference on Earthquake Engineering. Lisbon, Portugal*.

Della Corte, G., De Matteis, G., Landolfo, R. and Mazzolani, F. (2002), "Seismic analysis of MR steel frames based on refined hysteretic models of connections", *J. Constr. Steel Res.*, **58**(10), 1331-1345. https://doi.org/10.1016/S0143-974X(02)00014-7.

Diaferio, M. (2018), "Performance of seismic shear panels under near-field motions", *Int. J. Eng. Technol.,* **7**(2), 196-200.

Diaferio, M. and Foti, D. (2016), "Mechanical behavior of buildings subjected to impulsive motions", *Bull. Earthq. Eng.*, **14**(3), 849-862. https://doi.org/10.1007/s10518-015-9848-5.

Díaz, C., Martí, P., Victoria, M. and Querin, O.M. (2011), "Review on the modelling of joint behaviour in steel frames", *J. Constr. Steel Res.,* **67**(5), 741-758. https://doi.org/10.1016/j.jcsr.2010.12.014.

Elnashai, A.S. and Elghazouli, A. (1994), "Seismic behaviour of semi-rigid steel frames", *J. Constr. Steel Res.*, **29**(1-3), 149-174. https://doi.org/10.1016/0143-974X(94)90060-4.

Fang, C., Izzuddin, B., Elghazouli, A. and Nethercot, D. (2013), "Modeling of semi-rigid beam-to-column steel joints under extreme loading", *Front. Struct. Civil Eng.,* **7**(3), 245-263. https://doi.org/10.1007/s11709-013-0215-9.

Faridmehr, I., Tahir, M.M. and Lahmer, T. (2016), "Classification System for Semi-Rigid Beam-to-Column Connections", *Latin Am. J. Solids Struct.,* **13**(11), 2152-2175. https://doi.org/10.1590/1679-78252595.

Faridmehr, I., Tahir, M.M., Lahmer, T. and Osman, M.H. (2017), "Seismic performance of steel frames with semirigid connections", *J. Eng.*, **2017**.

Fathi, M., Daneshjoo, F. and Melchers, R. (2006), "A method for determining the behaviour factor of moment-resisting steel frames with semi-rigid connections", *Eng. Struct.*, **28**(4), 514-531. https://doi.org/10.1016/j.engstruct.2005.09.006.

Feizi, M.G., Mojtahedi, A. and Nourani, V. (2015), "Effect of semi-rigid connections in improvement of seismic performance of steel moment-resisting frames", *Steel Compos. Struct.*, **19**(2), 467-484. https://doi.org/10.12989/scs.2015.19.2.467.

FEMA-P695 (2009), *Quantification of building seismic performance factors*, Federal Emergency Management Agency

Foti, D. (2014), "On the seismic response of protected and unprotected middle-rise steel frames in far-field and near-field areas", *Shock Vibration*, **2014**. https://doi.org/10.1155/2014/393870.

Foti, D. (2014), "Response of frames seismically protected with passive systems in near-field areas", *Int. J. Struct. Eng.*, **5**(4), 326-345.

Foti, D. (2015), "Local ground effects in near-field and far-field areas on seismically protected buildings", *Soil Dynam, Earthq, Eng.*, **74**, 14-24. https://doi.org/10.1016/j.soildyn.2015.03.005.

Frye, M.J. and Morris, G.A. (1975), "Analysis of flexibly connected steel frames", *Canadian J. Civil Eng.*, **2**(3), 280-291. https://doi.org/10.1139/l75-026.

Hall, J.F., Heaton, T.H., Halling, M.W. and Wald, D.J. (1995), "Near-source ground motion and its effects on flexible buildings", *Earthq. Spectra*. **11**(4), 569-605. https://doi.org/10.1193/1.1585828.

Heaton, T.H., Hall, J.F., Wald, D.J. and Halling, M.W. (1995), "Response of high-rise and base-isolated buildings to a hypothetical Mw 7.0 blind thrust earthquake", *Science*. **267**(5195), 206-211. DOI: 10.1126/science.267.5195.206.

Housner, G. and Trifunac, M. (1967), "Analysis of accelerograms—Parkfield earthquake", *Bull. Seismol. Soc. Am.*, **57**(6), 1193-1220.

Huang, C.-T. (2003), "Considerations of multimode structural response for near-field earthquakes", *J. Eng. Mech.*, **129**(4), 458-467. https://doi.org/10.1061/(ASCE)0733-9399(2003)129:4(458).

IS-800 (2007), *General Construction in Steel-Code of Practice (Third Revision)*Bureau of Indian Standards, New Delhi.

IS-875 (1987), *Part 1: Dead loads — unit weights of building materials and stored materials* Bureau of Indian Standards, New Delhi.

IS-1893 (2016), *Criteria for earthquake resistant design of structures, Part 1 General Provisions and Buildings (Sixth Revision)*, Bureau of Indian Standards, New Delhi.

Kalkan, E. and Kunnath, S.K. (2006), “Effects of fling step and forward directivity on seismic response of buildings”, *Earthq. Spectra*. **22**(2), 367-390. https://doi.org/10.1193/1.2192560.

Kishi, N. and Chen, W.-F. (1990), “Moment-rotation relations of semirigid connections with angles”, *J. Struct. Eng*., **116**(7), 1813-1834. https://doi.org/10.1061/(ASCE)0733-9445(1990)116:7(1813).

Kitipomchai, S., Al-Bermani, F.G. and Chan, S.L. (1990), “Elasto-plastic finite element models for angle steel frames”, *J. Struct. Eng*., **116**(10), 2567-2581. https://doi.org/10.1061/(ASCE)0733-9445(1990)116:10(2567).

Lemonis, M. (2018), “Steel moment resisting frames with both joint and beam dissipation zones”, *J. Constr. Steel Res*., **147** 224-235. https://doi.org/10.1016/j.jcsr.2018.03.020.

Li, S. and Xie, L.l. (2007), “Progress and trend on near-field problems in civil engineering”, *Acta Seismologica Sinica*, **20**(1), 105-114. https://doi.org/10.1007/s11589-007-0105-0.

Liu, Y., Xu, L. and Grierson, D.E. (2008), “Compound-element modeling accounting for semi-rigid connections and member plasticity”, *Eng. Struct.,* **30**(5), 1292-1307. https://doi.org/10.1016/j.engstruct.2007.07.026.

Lui, E. and Chen, W. (1987), “Steel frame analysis with flexible joints”, *J. Constr. Steel Res.*, **8**, 161-202. https://doi.org/10.1016/0143-974X(87)90058-7.

Mahmoud, H.N., Elnashai, A.S., Spencer Jr, B.F., Kwon, O.S. and Bennier, D.J. (2013), “Hybrid simulation for earthquake response of semirigid partial-strength steel frames”, *J. Struct. Eng.*, **139**(7), 1134-1148. https://doi.org/10.1061/(ASCE)ST.1943-541X.0000721.

Malhotra, P.K. (1999), “Response of buildings to near-field pulse-like ground motions”, *Earthq. Eng. Struct. D*., **28**(11), 1309-1326. https://doi.org/10.1002/(SICI)1096-9845(199911)28:11<1309::AID-EQE868>3.0.CO;2-U.

Mavroeidis, G., Dong, G. and Papageorgiou, A. (2004), “Near-fault ground motions, and the response of elastic and inelastic single-degree-of-freedom (SDOF) systems”, *Earthq. Eng. Struct. D*., **33**(9), 1023-1049. https://doi.org/10.1002/eqe.391.

Mukhopadhyay, S. and Gupta, V.K. (2013), “Directivity pulses in near-fault ground motions—I: Identification, extraction and modeling”, *Soil Dynam. Earthq. Eng*., **50,** 1-15. https://doi.org/10.1016/j.soildyn.2013.02.017.

Mukhopadhyay, S. and Gupta, V.K. (2013), “Directivity pulses in near-fault ground motions—II: Estimation of pulse parameters”, *Soil Dynam. Earthq. Eng*., **50,** 38-52. https://doi.org/10.1016/j.soildyn.2013.02.019.

Nader, M. and Astaneh, A. (1991), “Dynamic behavior of flexible, semirigid and rigid steel frames”, *J. Constr. Steel Res*., **18**(3), 179-192. https://doi.org/10.1016/0143-974X(91)90024-U.

Najdian, M. and Izadinia, M. (2012). “Evaluation of seismic behavior on steel frames with TSW semi-rigid connections under the nonlinear time history analysis”, *Appl. Mech. Mater*., **166-169**, *https://doi.org/10.4028/www.scientific.net/AMM.166-169.2083.*

SAP2000v21 (2019), “Integrated Software for Structural Analysis and Design”, *Computers and structures Inc, Berkeley*, *CA*, *USA*.

Sehhati, R., Rodriguez-Marek, A., ElGawady, M. and Cofer, W.F. (2011), “Effects of near-fault ground motions and equivalent pulses on multi-story structures”, *Eng. Struct*., **33**(3), 767-779. https://doi.org/10.1016/j.engstruct.2010.11.032.

Shahbazi, S., Mansouri, I., Hu, J.W., Sam Daliri, N. and Karami, A. (2019), “Seismic response of steel SMFs subjected to vertical components of far-and near-field earthquakes with forward directivity effects”, *Adv. Civil Eng.,* **2019**.

Sharma, V., Shrimali, M., Bharti, S. and Datta, T. (2019), “Seismic energy dissipation in semi-rigid connected steel frames”, *Proceedings of the 16th World Conference on Seismic Isolation, Energy Dissipation and Active Vibration Control of Structures*, Saint Petersburg, Russia.

Somerville, P.G., Smith, N.F., Graves, R.W. and Abrahamson, N.A. (1997), “Modification of empirical strong ground motion attenuation relations to include the amplitude and duration effects of rupture directivity”, *Seismol. Res. Lett*., **68**(1), 199-222. https://doi.org/10.1785/gssrl.68.1.199.

Stamatopoulos, G.N. (2014), “Seismic response of steel frames considering the hysteretic behaviour of the semi-rigid supports”, *Int. J. Steel Struct*., **14**(3), 609-618. https://doi.org/10.1007/s13296-014-3019-4.

Wang, G.Q., Zhou, X.Y., Zhang, P.Z. and Igel, H. (2002), “Characteristics of amplitude and duration for near fault strong ground motion from the 1999 Chi-Chi, Taiwan earthquake”, *Soil Dynam. Earthq. Eng*., **22**(1), 73-96. https://doi.org/10.1016/S0267-7261(01)00047-1.

Yadav, K.K. and Gupta, V.K. (2017), “Near-fault fling-step ground motions: Characteristics and simulation”, *Soil Dynam. Earthq. Eng*., **101,** 90-104. https://doi.org/10.1016/j.soildyn.2017.06.022.

CC